Wave Coupling and Nonlinear Interactions in the Atmospheres of Earth and Mars

Author:

Jeffrey M. Forbes

Affiliation:

Smead Aerospace Engineering Sciences, University of Colorado, Boulder, CO, 80309

Correspondence author:

Jeffrey M. Forbes

E-mail: forbes@colorado.edu

This paper reviews recent progress on the topic of vertical wave coupling in the atmospheres of Earth and Mars with particular emphasis on (1) nonlinear interactions between planetary waves and solar thermal tides, and on (2) identifying the secondary waves produced by such interactions in satellite-based observations. The secondary waves produce temporal and longitudinal variability that would not otherwise exist in the absence of wave-wave interactions, and thus add to the complexity of atmospheric dynamics at both planets. At Earth, this has implications for re-entry predictions and ionospheric variability, which translates to loss of integrity in communications, navigation and tracking systems. At Mars, atmospheric density predictions in support of aerobraking operations are impacted.

Abstract

1. Introduction

1.1 Overview of Wave Coupling

In planetary atmospheres, propagating waves often constitute the primary mechanism by which energy and momentum are transferred from one region to another. The relevant wave types include gravity or buoyancy waves (GW); thermal tides with periods that are subharmonics of the planetary rotation period; and planetary waves (PW) with periods that are several times the planet's rotation period. In 2002 a tutorial-level review of wave coupling in the atmospheres of Earth, Mars and Venus was provided [1] that covered all of these wave types. At that time, the importance of interactions between these wave types was appreciated, but observational evidence, theory and modeling were not well developed. This continues to be true for the interactions between GW and larger-scale waves such as tides and PW. However, some progress has been made with respect to PW-tide interactions in the atmospheres of Earth and Mars. It is the purpose of this paper to review recent advances on this topic.

The atmospheres of Earth and Mars are dynamically similar in many ways since they both receive strong forcing due to absorption of solar radiation, and their rotation rates are nearly the same: 2π day^{-1} for Earth and 2π sol^{-1} for Mars, where 1 day = 24 h and 1 sol = 23.5 h. While Earth's planetary diameter is about 12,756 km, that of Mars is 6794 km. Furthermore, their accelerations due to gravity are 9.8 ms^{-2} (3.73 ms^{-2}) and surface pressures are 1000 mb (6 mb) for Earth (Mars). Despite these vastly different surface pressures, the temperature structures and gravitational accelerations of both planets are such that the densities and pressures of the atmospheres of Earth and Mars are about the same at an altitude of about 110 km. Up to this altitude, mixing by various dynamical processes including turbulence keeps relative chemical compositions constant with height: for Mars, roughly 95% CO_2 and 3% N_2, and 21% O_2 and 78% N_2 for Earth. Above this altitude, densities become sufficiently low that molecular diffusion dominates and various chemical species vary with height according to their respective atomic and molecular weights. This, combined with the fact that ultraviolet and extreme ultraviolet solar radiation photo-dissociate O_2 and CO_2, results in O being the dominant species above about 160-200 km in both atmospheres until lighter species such as He and H take over. The altitude of 110 km is thus sometimes called the *turbopause*, or the separation between the *homosphere* (below) and *heterosphere* (above). It is also not too far above the 90-100 km altitude where Earth's intrinsic magnetic field begins to exert influence on atmospheric dynamics. [Mars does not have an intrinsic global magnetic field, but it does have crustal magnetic anomalies whose effects are felt at high altitudes.] For this reason, and because there is no universally-accepted nomenclature, it is convenient for present purposes to separate the atmospheres of Earth and Mars into a *lower atmosphere* and *upper atmosphere* where the 110-km turbopause demarcates the two regimes.

The reader is now referred to Figure 1 for a broad overview of wave coupling and related processes in the atmospheres of Earth and Mars. At Earth, periodic absorption of solar radiation in local time (LT) and longitude by tropospheric H_2O and stratospheric O_3 as well as latent heat release in deep tropical clouds excites a spectrum of thermal tides. Surface topography and unstable shear flows excite planetary waves (PW) and gravity waves (GW). PW are either quasi-stationary (i.e., they do not propagate zonally or do so at very slow speeds) or are oscillations at periods primarily near 2, 5, 6.5, 10, and 16 days, and occasionally at other

periods. They are often related to natural quasi-resonances in the atmosphere, but can sometimes arise through, or be amplified by, instabilities that are enabled by mean wind shears forced by solar inputs and momentum deposited by GWs. Other prominent waves that vertically couple Earth's atmospheric regions are equatorially-trapped "ultra-fast Kelvin waves (UFKW)" with periods between about 2 and 5 days. UFKW are excited by latent heating associated with deep tropical convection in the troposphere, and along with some tides that are excited by latent heat release, essentially carry the imprint of tropical troposphere spatial-temporal variability into the upper atmosphere. Vertically-propagating waves grow exponentially with height into the more rarified atmosphere, ultimately achieving large amplitudes, mainly in the dissipative region between about 100 and 150 km. Some fraction of the waves penetrates all the way to the base of the exosphere (ca. 500-600 km, Earth; 300 km, Mars). Along the way, nonlinear interactions between different wave types occur, modifying the interacting waves and giving rise to secondary waves which add to the spatial-temporal complexity of the dynamics.

The situation is not too different at Mars. GW and stationary PW are generated by flow over orography. Traveling PW with periods between about 5 and 20 days exist at Mars,

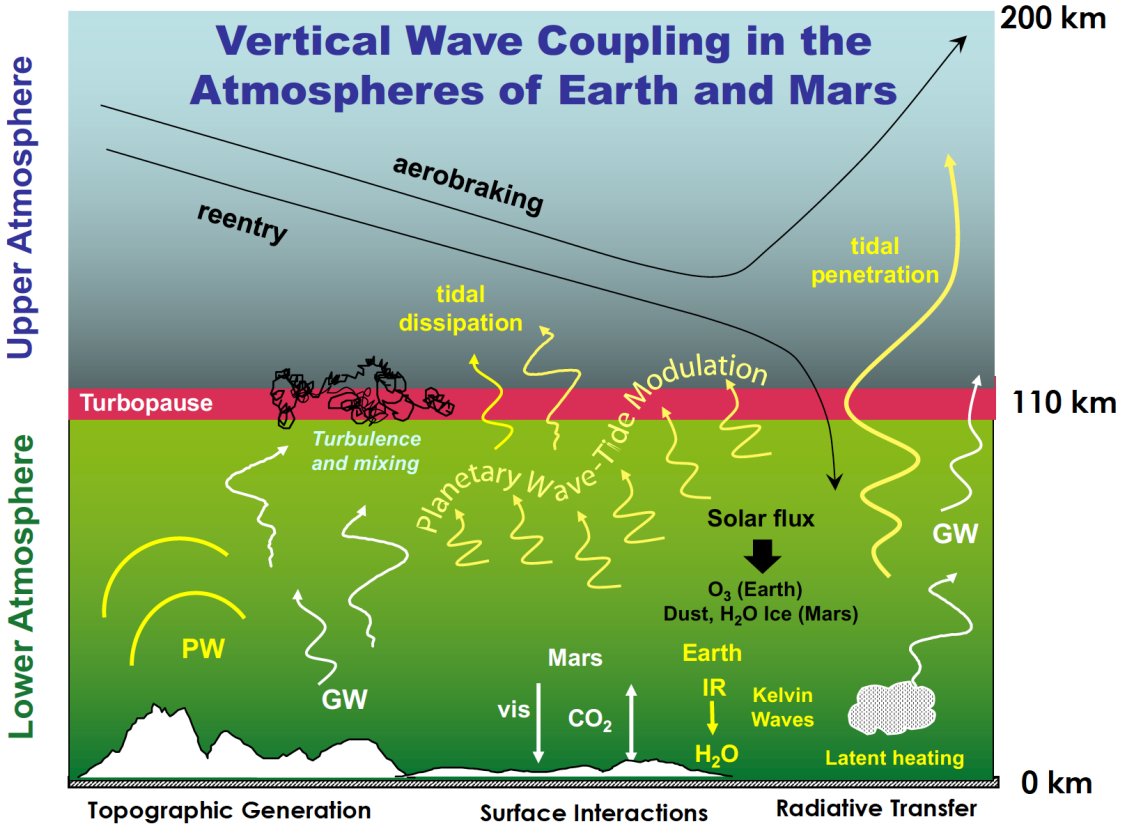

Figure 1. Schematic of wave generation, vertical coupling and related processes in the atmospheres of Earth and Mars. Also shown are the trajectories of reentering (Earth) and orbiting (Mars) objects, the latter in *aerobraking* mode using drag to contract the orbit from elliptical to circular.

although we are less certain about their origins and predominant periods as we are for Earth. H_2O and O_3 are rare in Mars atmosphere, but heating due to solar infrared radiation absorption by dust and water ice, and visible radiation absorption by dust play similar roles in heating Mars' atmosphere as H_2O and O_3 at Earth. Visible radiation also heats Mars' surface, which radiates in the infrared, and through exchange with the CO_2 atmosphere, this diurnally-varying heat source also excites thermal tides. At both Earth and Mars, surface topography and land-sea differences (at Earth) modulate tidal heating and give rise to longitudinally-varying tidal heat sources and responses.

Vertically-propagating tides reach their maximum amplitudes between about 100-140 km due to molecular dissipation. The associated tidal density perturbations have practical consequences at both planets. For instance, at Earth the surface impact locations of uncontrolled re-entering objects (i.e., debris) vary significantly depending on the specific latitude, longitude and local time of reentry [2] due to the ambient tidal density variations. At Mars, satellite missions are initially "captured" into highly elliptical orbits around the planet. However, science missions often call for relatively low-altitude circular orbits. Aerobraking is a fuel-saving maneuver used to contract satellite orbits after initial insertion into a planetary atmosphere. It consists of dipping into atmospheric altitudes where atmospheric drag is sufficiently large to modify and eventually "circularize" the orbit, which can take several months to accomplish. The rapidity and confidence with which this can be done largely depends on knowledge of the orbit-to-orbit density variability due to vertically-propagating tides [3].

The main objective of this paper is to convey how PW nonlinearly interact with (or modulate) vertically-propagating tides, and generate secondary waves that add to the complexity of the dynamics from observational, theoretical and modeling perspectives. Before doing this, in the following sections tidal and PW nomenclatures, and mathematical formulations regarding PW-tide interactions, are introduced.

1.2 Tidal and PW Nomenclatures

A particular notation has been widely adopted to describe the different components of the tidal spectrum. The mathematical form $A_{n,s} = \cos(n\Omega t + s\lambda - \varphi_{n,s})$ represents a tidal oscillation in any atmospheric variable, where $A_{n,s}$ is the amplitude; n = 1, 2, 3 refers to diurnal, semidiurnal and terdiurnal (periods of 24h, 12h, 8h, respectively); $\Omega = 2\pi/24h$; s is the zonal wavenumber; λ is longitude; and $\varphi_{n,s}$ is the phase (time of amplitude maximum at $\lambda = 0$). A tide that migrates with the westward motion of the Sun to a ground-based observer corresponds to $s = n$ and appears the same at all longitudes. Longitudinal variability projects onto a range of wavenumbers $s \neq n$ at each frequency. Furthermore, converting the above expression for $A_{n,s}$ to the local time frame, $A_{n,s} = \cos(n\Omega t_{LT} + (s-n)\lambda - \varphi_{n,s})$, we see that from a quasi-Sun-synchronous ($t_{LT} \approx const$) perspective (i.e., a high-inclination satellite orbit) that a tide with zonal wavenumber s and period $n\Omega$ appears as an $|s-n|$ longitudinal variation. Traveling PW are expressed as $A_{n,s} = \cos(\delta\Omega t + m\lambda - \varphi_{n,s})$ where $\delta < 1$ and m is an integer zonal wavenumber.

In this context we utilize the notation *DWs* or *DEs* to denote a westward or eastward-propagating diurnal tide, respectively, with zonal wavenumber = s. For semidiurnal and terdiurnal oscillations *'S'* and *'T'* respectively replaces *'D'*. The zonally-symmetric oscillations are denoted D0, S0, T0. At Earth, the most prominent vertically-propagating tidal components known to penetrate well above about 100 km are D0, DE2, DE3, D0, SW2, SE1, SE2, SE3, TW3 [4-6]; at Mars, D0, DE1, DE2, DE3, S0, SW2, SE1, SE2, SE3 [e.g., 7,8].

(i) $\frac{\partial u}{\partial t}+\frac{u}{a\cos\theta}\frac{\partial u}{\partial \lambda}+\ldots$

(ii) $\frac{\partial u_0}{\partial t}+\frac{u_0}{a\cos\theta}\frac{\partial u_0}{\partial \lambda}+\ldots$

(iii) $\frac{\partial u'}{\partial t}+\frac{u_0}{a\cos\theta}\frac{\partial u'}{\partial \lambda}+\frac{u'}{a\cos\theta}\frac{\partial u_0}{\partial \lambda}+\ldots$ Source S''

(iv) $\frac{\partial u''}{\partial t}+\frac{u_0}{a\cos\theta}\frac{\partial u''}{\partial \lambda}+\frac{u''}{a\cos\theta}\frac{\partial u_0}{\partial \lambda}\ldots\ldots=\frac{u'}{a\cos\theta}\frac{\partial u'}{\partial \lambda}$

$$S'=\sum_{s=-k}^{s=+k}\sum_{n=1}^{N}A_{n,s}(z,\theta)\cos\left(n\Omega t+s\lambda-\phi_{n,s}(z,\theta)\right)$$

$\Omega=\frac{2\pi}{24h}$ t = time

$n=1$ (diurnal) λ = longitude

$n=2$ (semidiurnal) s = zonal wavenumber

$n=3$ (terdiurnal) z = altitude

θ = latitude

Figure 2. Hierarchy of perturbation equations (left) and representation of first-order source term (right).

2. PW-Tide Interactions and Secondary Waves

Nonlinear interaction between a tide and a PW is conventionally viewed in terms of the longer-period wave (PW) modulating the shorter-period wave (tide). It is thought to occur through a nonlinear interaction that results in the generation of "sum" and "difference" secondary waves [9-11]. In fact, the interaction between a PW with frequency $\delta\Omega$ and zonal wavenumber m, $\cos(\delta\Omega t + m\lambda)$, and a tide with frequency $n\Omega$ and zonal wavenumber s, $\cos(n\Omega t + s\lambda)$, thus yields sum and difference waves with frequencies $n\Omega \pm \delta\Omega$ and zonal wavenumbers $s \pm m$, respectively. In the spectrum of a time series, long-period PW ($\delta \ll 1$) appear as two sideband peaks on either side of the main tidal peak at frequency $n\Omega$. To understand the origin of the above rather simple concept, consider that the large-scale dynamics of the atmosphere is represented by the horizontal momentum, continuity and thermal energy equations, the hydrostatic law, and the equation of state. The equations contain nonlinear terms, and as one representative example, consider the first nonlinear terms in the zonal (east-west) momentum equation where u = eastward velocity, a = radius of the earth, θ = latitude and λ = longitude; see (i) in Figure 2. Now consider a perturbation expansion solution $u = u_0 + \varepsilon u' + \varepsilon^2 u'' + \cdots\cdots$ where the system of equations is forced by some source term $S = S_0 + \varepsilon S' + \varepsilon^2 S'' + \cdots\cdots$. Introducing these expressions into the system of equations and gathering like powers of ε, we have a "zeroth order" set of equations ((ii) in Figure 2) that can be solved for the zonal- and diurnal-mean atmospheric state, i.e., $u_0, T_0, \rho_0,\ etc.$, all a function of height (z) and latitude (θ) provided the $z-\theta$ distribution of S_0 is

known. Knowing the sources S' (i.e., tidal and planetary wave forcing as expressed in Figure 2) and the zonal mean state, the equations in the form (iii) in Figure 2 can be solved for the perturbation fields $u', T', \rho', etc.$, in complex form, each unknown corresponding to an individual, linearly independent tide or PW depending on the forcing that is chosen. This step is exactly what is done in global linearized models of atmospheric tides and PW such as the Global-Scale Wave Model (GSWM; 12-17), except that the zonal mean state is specified through available empirical models and/or observational data, rather than solving the zeroth-order system of equations.

Finally, knowing any two tide and/or PW solutions (i.e. primary waves), as well as the zonal mean atmospheric state, the sources S'' for the sum and difference secondary waves can be formulated, and as expressed in (iv) of Figure 2, a second-order perturbation set of equations can be solved, one for each secondary wave that results from nonlinear interaction between the two primary waves. Self-interactions for each primary wave are neglected [10, 18]. Note that the source term S'' for the linear set of equations in u'' represented in Figure 2 consists of terms that arise as products of first-order wave quantities, e.g., u'. In the present context, one of the first-order ("primary") waves is a PW expressed in the form $\cos(\delta\Omega t + m\lambda)$, and the other primary wave is a tide, expressed in the form $\cos(n\Omega t + s\lambda)$. This leads to two source terms and two sets of equations in u'', one for each secondary wave produced by nonlinear interaction between the primary waves [9-11]. The secondary waves have frequencies and zonal wavenumbers that are the "sum" and "differences" of the primary waves, i.e., $SW^+ \propto \cos[(n+\delta)\Omega t + (s+m)\lambda]$ and $SW^- \propto \cos[(n-\delta)\Omega t + (s-m)\lambda]$. As described below, we can also use this kind of framework to identify nonlinear wave-wave interactions in observations, and the secondary waves resulting from such interactions.

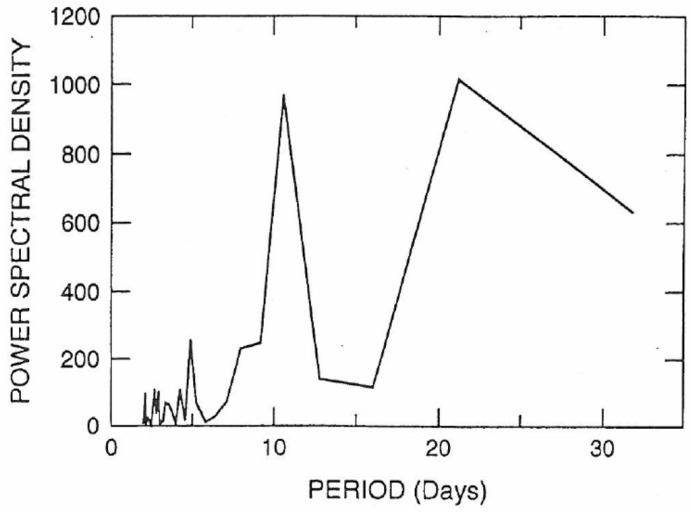

Figure 3. Power spectrum of daily semidiurnal meridional wind amplitudes measured over Obninsk, Russia (54ºN) during January-February, 1979, illustrating quasi-6-day, 10-day and 21-day modulations of the semidiurnal tide. The 10-day semidiurnal modulation amounted to a roughly ±30% variation about the mean amplitude [19].

3. Evidence for PW-Tide Interactions from Observations at Earth's Surface

For Earth, there is ground-based observational evidence that PW modulate atmospheric tides and that the interactions between planetary waves and tides may be a major source of tidal variability in the upper atmosphere. One example is shown in Figure 3, which provides evidence for quasi-6-day, 10-day and 21-day modulations of semidiurnal tidal winds measured by the meteor radar method near 95 km altitude over Obninsk, Russia (54ºN). The 10-day semidiurnal modulation amounted to about ±30% variation about the mean amplitude [19]. An example illustrating ~ ±20% quasi-2-day wave (QTDW) modulation of the semidiurnal tide using the meteor radar at Sheffield, UK (53ºN), is provided in Figure 4 [20]. Spectral analysis of the time series (not shown) yields peaks at periods of 9.6h and 16.0h in addition to 12.0h, which leads one to conclude that these are likely secondary waves due to interaction between the QTDW with m = 3 and SW2 (n = 2, s = 2): that is, SW^+ is a 9.6-hour wave (n = 2.5) with s = +5 (westward-propagating) and SW^- is a 16-hour wave (n = 1.5) with s = -1 (eastward-propagating). Such a conclusion has been drawn before under similar circumstances [21-25]; however, none of the zonal wavenumbers are determinable from observations at a single geographic location.

The above examples bring to light the difficulty of gaining a global perspective of PW-tide interactions. The observations really required to unambiguously quantify PW-tide interactions in the time domain can only originate in ground-based measurements, but the existing distribution of ground-based sites is inadequate to provide a global perspective. The temporal sampling provided by satellite measurements, on the other hand, is inadequate to derive tides over time scales short compared with PW periods; therefore, it would seem impossible to provide evidence for PW-tide interactions from space. However, a method has been developed to infer and quantify PW-tide interactions from space, and thus provide a global perspective, albeit involving multiple possible mathematical solutions in terms identifying the tidal primary waves. The following section describes this methodology, and provides examples from both Earth and Mars.

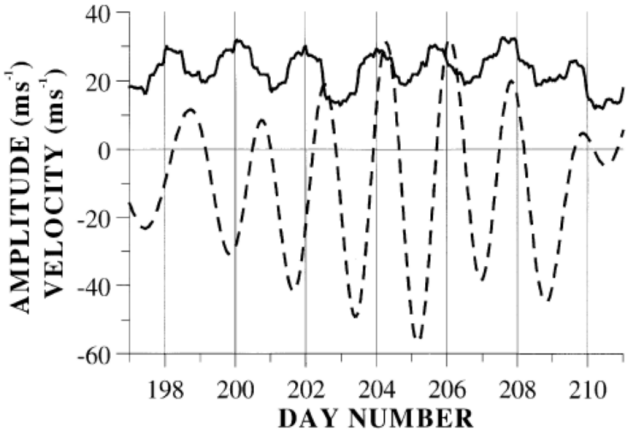

Figure 4. Meteor radar wind observations near 95 km altitude over Sheffield, UK, 16-29 July, 1993 [20]. The dashed line illustrates the quasi-two-day oscillation in low-pass filtered winds. The solid line illustrates the ~ ±20% quasi-two-day modulation of the semidiurnal tidal winds.

4. Satellite-Based Observations of PW-Tide Interactions

4.1 PW, Tides and Secondary Waves as Observed from Space

A method has been developed that provides evidence for the existence of PW-tide interactions, and that can be used to quantify the longitudinal variability added by the presence of secondary waves. This methodology was originally derived to explain density variability in the lower thermosphere of Mars [25-28], but later applied to the quasi-two-day wave at Earth [29-31]. The methodology consists of ordering data in pseudo-longitude, the traditional longitude incremented by 360° times the number of Earth revolutions since a given time. This arrangement eliminates the fictitious discontinuity at 0/360° longitude. The mathematical description of tides and PW remains unchanged. The time-longitude dependence of a tide thus remains $\cos(n\Omega t + s\lambda_p)$ where λ_p is now the pseudo longitude. The same notation applies to a PW: $\cos(\delta\Omega t + m\lambda_p)$ describes a single PW having a frequency δ (per day) and a zonal wavenumber m; e.g., in the case of a 2-day wave, $\delta = 0.5$. The interaction of a tide and PW in the above forms yields secondary waves with frequencies equal to $(n \pm \delta)\Omega$ and zonal wavenumbers equal to $s \pm m$. When sampled at a nearly constant local time (i.e., quasi-sun-synchronous satellite like TIMED), a tide appears as a wave in the form $\cos(n\Omega t_{LT} + (s-n)\lambda_p)$, a PW as $\cos(\delta\Omega t_{LT} + (m-\delta)\lambda_p)$, and secondary waves as $\cos[(n \pm \delta)\Omega t_{LT} + (s \pm m - n \mp \lambda_p)]$. These various spaced-based zonal wavenumbers ($k_s = s - n$, $m - \delta$ and $s \pm m - n \mp \delta$) for different existing tides, PWs and their secondary waves each contribute to the zonal variability in any atmospheric field.

4.2 Evidence for PW-tide Interactions from Earth-Orbiting Satellites

Spectral analysis of a given time series of space-based measurements as described above, can reveal the dominant values of $k_s = s - n,\ m - \delta$ and $s \pm m - n \mp \delta$, and subsequently the dominant tides, PWs and any PW-tide modulations. Note that tides appear as integers, and one cannot differentiate between a PW and the PW modulation of a migrating tide ($s - n = 0$). In Figure 5 we show an example [32], which illustrates a pseudo-longitude spectrum of temperatures containing DE3, a 3.5-day UFKW, and the 2 secondary waves resulting from their interaction: SW^+ has a period of 0.77 days and zonal wavenumber s = -4, and SW^- has a period of 1.43 days and zonal wavenumber of s = -2. Although these secondary waves are not retrievable from normal time series analyses, they are identifiable in the pseudo-longitude spectrum due to the specificity of their space-based wavenumbers (k_s).

These authors [32] also demonstrate the existence of these waves near 260 km in densities measured by the GOCE satellite, and that the secondary waves contribute significantly to the total spatial-temporal variability of temperatures at 100 km and densities at 260 km. An example is provided in Figure 6, which illustrates latitude-longitude reconstructions of temperatures at 100 km based on the spectral peaks shown in Figure 5. The observed structure, averaged over 10 days and centered on DOY 160, is at the top. Also shown are the UFKW; sum of SW+ and SW-; longitudinal waves 1-4 (i.e., tides); waves 1-4 + UFKW; and the total reconstructed structure at the bottom, which replications the observed structure very well. This figure demonstrates how secondary waves add to the complexity of the dynamical system.

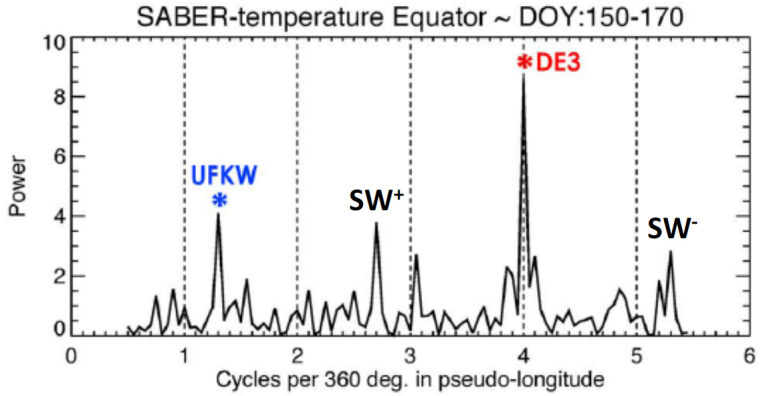

Figure 5. Pseudo-longitude spectrum of temperatures at 100 km measured by the SABER instrument on the TIMED (Thermosphere Ionosphere Mesosphere energetics and Dynamics) satellite during days 150-170 of 2011, illustrating DE3, the UFKW with period of 3.5 days and s = -1, and the secondary waves resulting from their interaction: SW^+ (k_s = 2.7) has a period of 0.77 days and s = -4, and SW^- (k_s = 5.3) has a period of 1.43 days and s = -2.

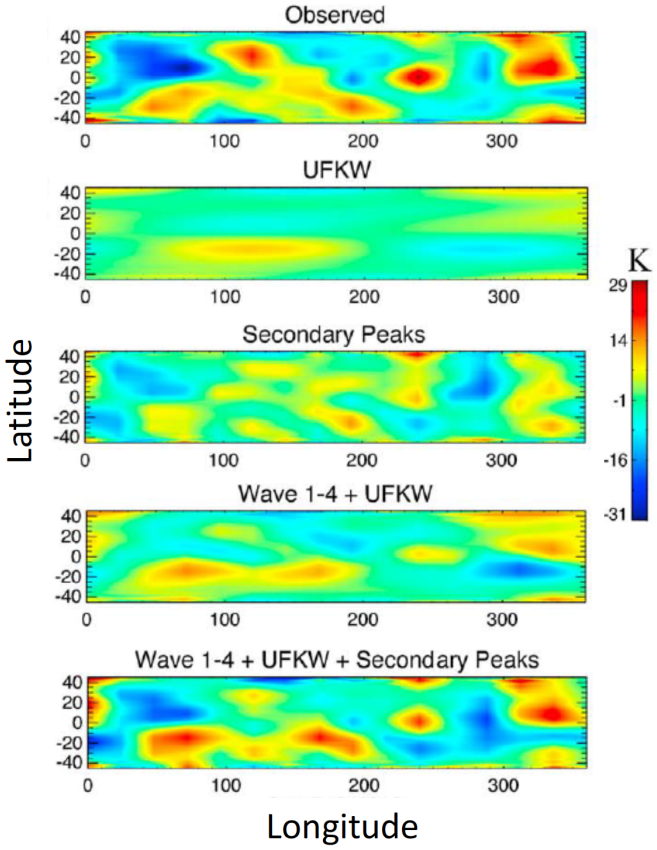

Figure 6. Latitude-longitude temperature reconstructions based on the spectral peaks in Figure 5. The observed structure, averaged over 10 days centered on DOY 160, is at the top. Also shown are the UFKW; SW^+ + SW^-; longitudinal waves 1-4 (i.e., tides); waves 1-4 + UFKW; and the total reconstructed structure at the bottom, which replications the observed structure very well [32].

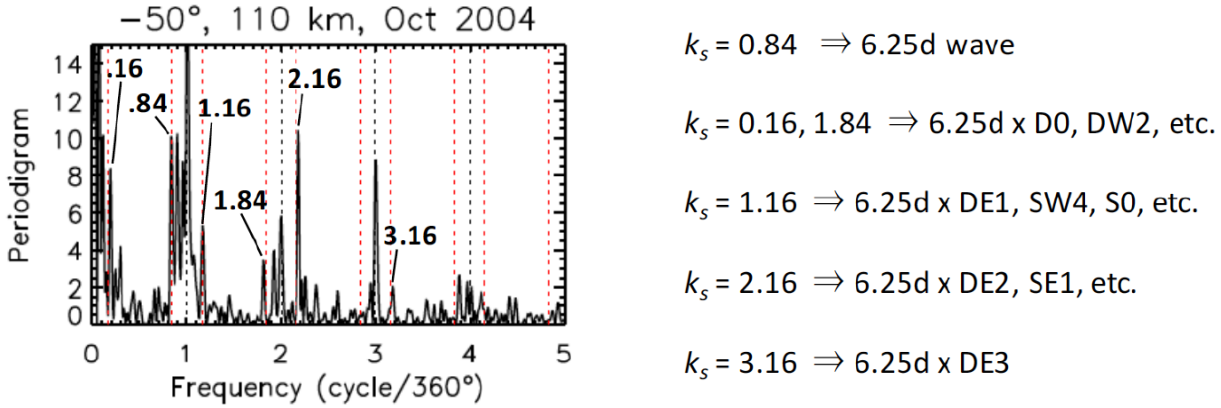

Figure 7. Pseudo-longitude spectrum of SABER temperatures at 110 km and -50° latitude during October 2004, illustrating the 6.25-day wave (k_s = 0.84) and various peaks corresponding to nonlinear interactions between the 6.25-day PW and various tides [33]. Note that for a given k_s value, there are multiple possible tidal primary waves.

An additional example that underscores the scope of the problem is provided in Figure 7 [33]. Figure 7 shows a pseudo-longitude spectrum for SABER temperatures at 110 km during October 2004, illustrating interactions between a 6.25-day wave and various tidal components, and the secondary wave peaks corresponding to the interactions between various tides and the 6.25-day wave. It is important to note that a given spectral peak can arise as a result of the 6.25-day wave and several tidal components; as an example, the k_s = 1.16 peak can arise from interaction of the 6.25-day wave and DE1, SW4, S0 or any tide that possesses a longitudinal wavenumber = 2 from a quasi-Sun-synchronous orbit. These authors demonstrate that the seasonal-latitudinal amplitude structure of the k_s = 1.16 amplitude is well-defined, and that amplitudes are comparable to the individual 60-day mean amplitudes of DE1, SW4, and S0 in the SABER data, and thus is of significant importance to the dynamics.

4.3 Evidence for PW-Tide Interactions from Mars-Orbiting Satellites

Evidence for wave coupling into the upper atmosphere of Mars mainly originates from accelerometers that measure atmospheric density in the 100-150 km region [34-37]; other in-situ observations [38, 39]; and numerical modeling [e.g., 7, 8, 37]. All of these studies focus on longitudinal variability attributable to non-migrating tides, and suffer from similar difficulties in terms of local time coverage as many Earth-orbiting satellites; that is, tides are poorly determined, and often over longer time scales than PW periods, and therefore present difficulties in terms of providing evidence for PW-tide modulation. However, there has been some success applying the methods described in Section 4.2 to Mars, which are now described.

PW-tide interactions at Mars were first detected in Mars Global Surveyor (MGS) and Mars Reconnaissance Orbiter (MRO) aerobraking density data [26]. The example to be shown here corresponds to MGS measurements. MGS aerobraking occurred in two phases. Phase I lasted for about 200 orbits, and periapsis (the closest the spacecraft comes to the planet) was located

between about 40°N–60°N and local solar time (LT) gradually increased from 1100h to 1600h. During Phase II spanning orbits 600-1200, periapsis moved from about 60ºN to the vicinity of the South Pole, while LT remained nearly constant at 1500 h. Since the pseudo longitude method described previously was designed for near-Sun-synchronous application, the search for PW-interactions was confined to Phase II.

The left panel of Figure 8 illustrates raw periapsis density measurements from MGS during the course of Phase II aerobraking in terms of percent density residuals from the longitude-mean at any given latitude, which amount to about ±40%. The right panel illustrates the reconstructed densities based on fits to longitudinal wavenumbers 1, 2 and 3. The reconstruction captures the salient features of the raw data very well, and exhibits a dominant wave-2 pattern which is mainly attributed to the presence of the DE1 tide in Mars atmosphere (i.e., a space based zonal wavenumber k_s = |s-n| = 2, where s = -1 and n = 1). However, this interpretation is somewhat misleading. Examination of the latitude vs. longitude structures of individual wavenumbers s = 1, 2, and 3 (not shown) all exhibit significant amplitudes in the range ±20%. We note the oscillations in density with time (or latitude), which represent the signature of PW modulation. These oscillations are present in all 3 wavenumbers to a significant degree, although some with different periods than others.

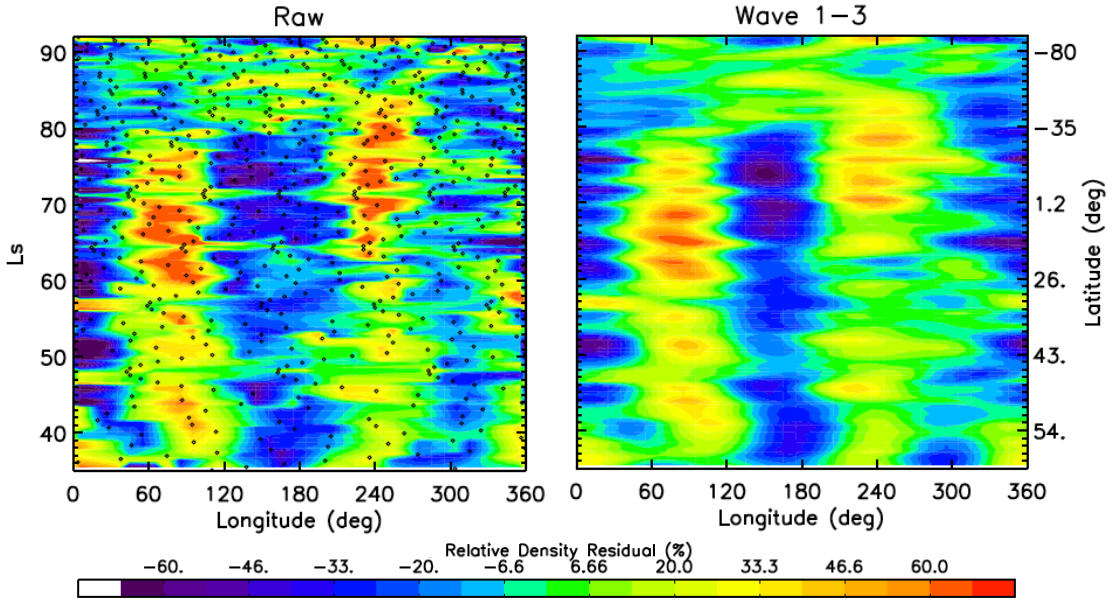

Figure 8. Left: Measured densities from MGS aerobraking in terms of percent differences from the longitude-mean at any given latitude. The dots indicate the location of periapsis and the density measurement. The existence of measurements at various longitudes at a given latitude are indicative of the planet rotating beneath the Sun-synchronous orbit. The y-axis on the left is in term of aerocentric longitude (Ls) with respect to the Sun, while the corresponding latitudes indicating the precession of periapsis from high latitudes in the Northern Hemisphere to high latitudes in the Southern Hemisphere are shown on the right-hand y-axis. Right: Reconstruction of the density pattern based on zonal wavenumber s = 1, 2 and 3 fits to the raw densities.

The temporal periodicities in the MGS densities were quantified using the method described in Section 4.2 [26], and the results are shown in Figure 9. At 25ºN, we see that the dominant PW period is 9 sols, that the largest PW variability is imposed on wave-3, and that statistically significant variability is imposed on waves 1 and 2. At 36ºS wave-1 is modulated by periods of 9, 18 and 27 sols, while wave-3 is modulated by 9-sol period. At 70ºS, wave-1 is modulated at 8-sol period. The complicating factor in all of this, of course, is that the most like tidal components associated with these wavenumbers are not unique: D0, SW1 for wave-1, DE1, S0 for wave-2, and DE2, SE1 for wave-3 [26]. Nevertheless, the evidence for PW-tide nonlinear interaction is present in the data, and is likely to account for much of the variability of tides in Mars' atmosphere. In other similar work, PW-tide interactions were quantified in temperature measurements between 15 and 80 km from Mars Climate Sounder (MCS) measurements on MRO [27].

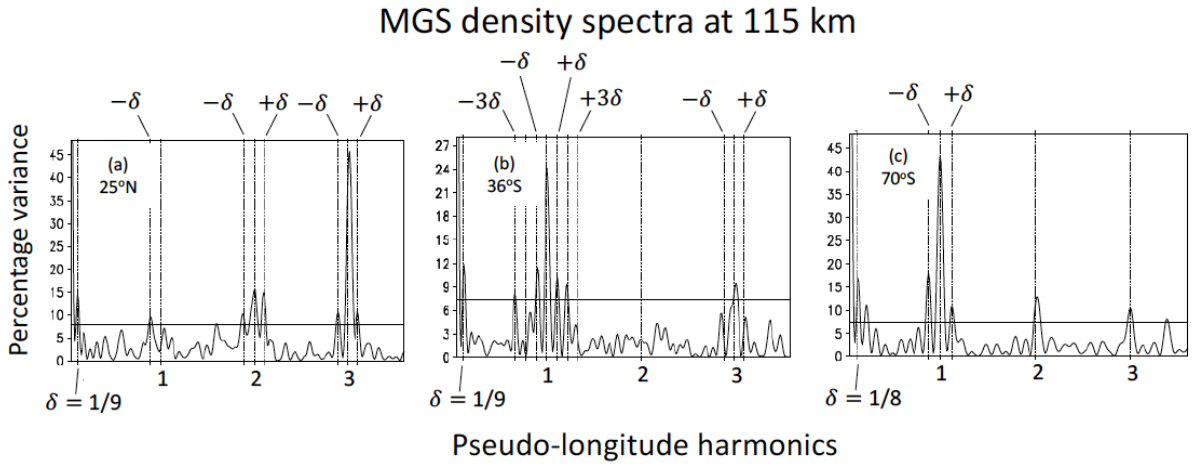

Figure 9. Pseudo-longitude spectra of MGS density measurements at 115 km at (a) 25ºN, (b) 36ºS, and (c) 70ºS. The dominant planetary wave frequency in each spectrum is represented by δ, or period $1/\delta$ in sols [26].

5. PW-Tide Interactions in Numerical Models

There are a few notable examples of numerical simulations that focus on PW-tide interactions in Earth's atmosphere, mostly using "whole atmosphere" general circulation models (GCMs). One landmark study [41] simulated the interaction between the QTDW and SW2 discussed in Section 3, and demonstrated that the two 9.6h and 16h secondary waves propagated as independent oscillations and penetrated well into the upper atmosphere. The same problem was more recently diagnosed with a quasi-nonlinear version of the GSWM [42]. Another GCM study [43] simulated the modulations of DE3 and DW1 by the 6.5-day wave, which produces secondary waves with respective periods and zonal wavenumbers of (20h, s = -2; 28h, s = -4) and (20h, s = 2; 28h s = 0). Tide-tide interactions conform to the same basic theory as outlined in this paper; for instance, simulations [44] show that DE3 and DW1 can interact to produce SE2 and SPW4 in Earth's upper atmosphere. Insofar as Mars is concerned, the only study [28] to address PW-tide interactions in a Mars

General Circulation Model demonstrated that tidal interactions with PW at periods of 2.2, 5, 9 and 19 sols produced a whole host of secondary waves with amplitudes of importance in the upper atmosphere.

The present paper has concentrated on tidal interactions with traveling planetary waves, i.e., those with non-zero frequency ($\delta = 0$ in prior equations). However, numerical simulations [e.g., 45-48] show that tidal interactions with stationary planetary waves (SPW) also produce secondary waves, both at the same frequency as the primary tide but with the sum and difference zonal wavenumbers determined by the SPW zonal wavenumber. Such interactions mainly occur within the 10-60 km altitude region at middle to high latitudes during local winter when the SPW are most prominent. For instance, consider the interaction between a SPW with zonal wavenumber s = 1 (SPW1) and the semidiurnal migrating tide (SW2). Mathematically, the SPW1-SW2 interaction gives rise to the "sum" and "difference" semidiurnal non-migrating tides SW1 and SW3:

$$\underset{\text{SW2}}{\cos(2\Omega t + 2\lambda)} \times \underset{\text{SPW1}}{\cos\lambda} \rightarrow \underset{\text{SW1}}{\cos(2\Omega t + \lambda)} + \underset{\text{SW3}}{\cos(2\Omega t + 3\lambda)}$$

which propagate globally and into the upper atmosphere above 100 km. Similarly, interaction between SPW1 and DW1 give rise to DW2 and D0, and migrating tide interactions with SPW2 give rise to S0, SW4 and DE1, DW3. Experimental evidence exists for some of these interactions [e.g., 49-52]. In Mars' atmosphere, SPW-tide interactions have been invoked to explain the presence of certain nonmigrating tides in GCM simulations [40].

A common feature among numerical simulations of PW-tide interactions so far is that the secondary waves propagate away from their sources as independent oscillations. Each secondary wave is affected differently by the background wind field depending on its zonal wavenumber and Doppler-shifted frequency. Therefore, at some distance from the source one of the sideband waves could be significantly larger than the other. Further, the two secondary waves do not seem to be excited with equal efficiency in these interactions, and the underlying reason is unknown.

6. Concluding Remarks

For Earth and Mars, we have a reasonable idea about the thermal tidal components and planetary waves that exert their influence on the upper atmosphere of these planets, at least in a climatological sense. An area of research where progress has been lacking is the short-term (days to weeks) variability of atmospheric tides, which is known to be significant based on ground-based observations. However, we are practically absent any idea about how tides vary globally on day-to-day or even weekly time scales. To be sure, significant variability likely arises in terms of the tidal sources, but also in terms of the propagation environment which includes global-scale waves. The main purpose of this review has been to document evidence for PW-tide interactions as a source for such variability, and to note the impacts of secondary waves resulting from these interactions on the upper atmospheres of Earth and Mars. The point to be made here is, modulation of tides by a PW introduces temporal and spatial complexity by virtue of the secondary waves, which have different periods and zonal wavenumbers than the primary waves. Since a given planetary wave can modulate several components of the tidal spectrum, each with a different period and zonal wavenumber, one can easily see how

complex the resultant tidal spectrum can become.

At Earth, much of the complexity noted above is expected to translate to the ionosphere through the electric fields generated by dynamo action of the wave wind fields enabled by presence of Earth's main magnetic field. However, since such a mechanism does not exist at Mars, the present review has largely omitted discussion of recent observational and modeling efforts that focus on the influence of PW-tide interactions on the ionospheres of Earth and Mars.

Lastly, this review was not meant to be a comprehensive survey of work and references relating to wave coupling at Earth and Mars. Rather, the reader is pointed to a few of the most relevant papers pertinent to the point at hand, with a view towards balance between the literatures of these two planets. Apologies are extended to those authors whose excellent works were not cited.

Acknowledgements.

This work was supported under Award AGS-1630177 from the U.S. National Science Foundation to the University of Colorado.

References

1. Forbes, J.M., Wave Coupling in Terrestrial Planetary Atmospheres, in Atmospheres in the Solar System: Comparative Aeronomy, Geophys. Monog. 130, 171-190, American Geophysical Union, 2002.

2. Leonard, J.M., J.M. Forbes, and G.H. Born, Impact of tidal density variability on orbital and reentry predictions, Space Weather, 10, S12003, doi:10.1029/ 2012SW000842, 2012.

3. Moudden, Y., and J.M. Forbes, Density prediction in Mars' aerobraking region, Space Weather, 13, 86–96, doi:10.1002/ 2014SW001121, 2015.

4. Forbes, J.M., Zhang, X., and S.L. Bruinsma, New perspectives on thermosphere tides - 2. Penetration to the upper thermosphere, Earth, Planets and Space, 66:122, doi:10.1186/1880-5981-66-122, 2014.

5. Oberheide, J., J.M. Forbes, K. Häusler, Q. Wu, and S.L. Bruinsma, Tropospheric tides from 80 to 400 km: Propagation, interannual variability, and solar cycle effects, J. Geophys. Res., 114, D00I05, doi:10.1029/ 2009JD012388, 2009.

6. Oberheide, J., J. M. Forbes, X. Zhang, and S. L. Bruinsma, Wave-driven variability in the ionosphere- thermosphere- mesosphere system from TIMED observations: What contributes to the "wave 4"?, J. Geophys. Res., 116, A01306, doi:10.1029/ 2010JA015911, 2011.

7. Angelats i Coll, M., F. Forget, M. A. Lo´pez-Valverde, P. L. Read, and S. R. Lewis, Upper atmosphere of Mars up to 120 km: Mars Global Surveyor accelerometer data analysis with the LMD general circulation model, J. Geophys. Res., 109, E01011, doi:10.1029/2003JE002163, 2004.

8. Forbes, J.M., Bridger, A.F.C., Bougher, S.W., Hagan, M.E., Hollingsworth, J.L., Keating, G.M., and J. Murphy, Nonmigrating tides in the thermosphere of Mars, J. Geophys. Res., 107(E11), 5113, doi:10.1029/2001JE001582, p. 23-1 to 23-12, 2002.

9. Spizzichino, A., Etude des interactions entre les différentes composantes du vent dans la haute atmosphere, Ann. Geophys., 25, 773-783, 1969.

10. Teitelbaum, H., F. Vial, A. H. Manson, R. Giraldez, and M. Massebeuf, Nonlinear interaction between the diurnal and semidiurnal tides: Terdiurnal and diurnal secondary waves, J. Atmos. Terr. Phys., 51, 627-634, 1989.

11. Teitelbaum, H., and F. Vial: On tidal variability induced by nonlinear interaction with planetary waves. J. Geophys. Res. 96, 14,169 - 14,178, 1991.

12.Hagan, M.E., J.M. Forbes, and F. Vial, On modeling migrating solar tides, Geophys. Res. Lett., 22, 893-896, 1995.

13. Hagan, M.E., Comparative Effects of Migrating Solar Sources on Tides in the Mesosphere and Lower Thermosphere, J. Geophys. Res., 101, 21213-21222, 1996.

14. Hagan, M.E., Burrage, M.D., Forbes, J.M., Hackney, J., Randel, W.J., and X.Zhang, GSWM-98: Results for migrating solar tides, J. Geophys. Res.,104(A4), 6813-6827, 1999.

15. Hagan, M. E. and J. M. Forbes, Migrating and nonmigrating diurnal tides in the middle and upper atmosphere excited by tropospheric latent heat release, J. Geophys. Res., 107(D24), 4754, doi: 10.1029/ 2001JD001236, 2002.

16. Hagan, M.E., and J.M. Forbes, Migrating and nonmigrating semidiurnal tides in the middle and upper atmosphere excited by tropospheric latent heat release, J. Geophys. Res., 108(A2), 1062, doi:10.1029/ 2002JA009466, 2003.

17. Zhang, X., J.M. Forbes, and M.E. Hagan, Longitudinal variation of tides in the MLT region: 1. Tides driven by tropospheric net radiative heating, J. Geophys. Res., 115, A06316, doi:10.1029/2009JA014897, 2010.

18. Hines, C.O., Internal gravity waves at ionospheric heights, Can. J. Phys., 38, 1441-1481, 1960.

19. Forbes, J.M., Tidal and Planetary Waves (A Tutorial), in the Upper Mesosphere and Lower Thermosphere: A Review of Experiment and Theory, edited by R.M. Johnson and T.L. Killeen, Geophysical Monograph Series, vol. 87, American Geophysical Union, 1995, pp. 356.

20. Beard, A. G., N. J. Mitchell, P. J. S. Williams, and M. Kunitake, Non-linear interactions between tides and planetary waves resulting in periodic tidal variability, J. Atmos.Sol. Terr. Phys., 61, 363–376, 1999.

21. Cevolani, G., and S. Kingsley, Non-linear effects on tidal and planetary waves in the lower thermosphere: Preliminary results, Adv. Space Res., 12(10), 77–80, 1992.

22. Manson, A.H., C.E. Meek, J.B. Gregory, and D.K. Chakrabarty (1982), Fluctuations in tidal (24–12h) characteristics and oscillations (5-25d) in the mesosphere and lower thermosphere at Saskatoon (52◦N, 107◦W), 1979–1981, Planet. Space Sci., 30, 1283.

23. Harris, T.J. and R.A. Vincent, The quasi-2-day wave observed in the equatorial middle atmosphere, J. Geophys. Res., 98, 10,481–10,490, 1993.

24. Thayaparan, T., W.K. Hocking, and J. MacDougal, Amplitude, phase and period variations of the quasi 2-day wave in the mesosphere/lower thermosphere over London, Ontario, during 1993 and 1994, J. Geophys. Res., 102, 9461–9478, 1997.

25. Thayaparan, T., W.K. Hocking, J. MacDougal, A.H. Manson, and C.E. Meek, Simultaneous observations of the 2-day wave at London Ontario (43◦N, 81◦W) and Saskatoon (52◦N, 107◦W) near 91 km altitude during the two years 1993 and 1994, Ann. Geophys., 15, 1324–1339, 1997b.

26. Moudden, Y., and J.M. Forbes, A new interpretation of Mars aerobraking variability: Planetary wave-tide interactions, J. Geophys. Res., 115, E09005, doi:10.1029/ 2009JE003542, 2010.

27. Moudden, Y., and J.M. Forbes, Simulated planetary wave-tide interactions in the atmosphere of Mars, J. Geophys. Res., 116, E01004, doi:10.1029/2010JE003698, 2011a.

28. Moudden, Y., and J.M. Forbes, First detection of wave interactions in the middle atmosphere of Mars, Geophys. Res . Lett., 38, L04202, doi:10.1029/2010GL045592, 2011.

29. Forbes, J.M., and Y. Moudden, Quasi-two-day wave-tide interactions as revealed in satellite observations, J. Geophys. Res., 117, D12110, doi:10.1029/2011JD017114, 2012.

30. Pedatella, N.M., and J.M. Forbes, The quasi 2-day wave and spatial-temporal variability of the OH emission and ionosphere, J. Geophys. Res., 117, A01320, doi:10.1029/2011JA017186, 2012.

31. Moudden, Y., and J.M. Forbes, Quasi-2-day wave structure, interannual variability, and tidal interactions during the 2002–2011 decade, J. Geophys. Res. Atmos., 119, 2241–2260, doi:10.1002/ 2013JD020563, 2014.

32. Gasperini, F., J.M. Forbes, E. N. Doornbos, and S. L. Bruinsma, Wave coupling between the lower and middle thermosphere as viewed from TIMED and GOCE, J. Geophys. Res. Space Physics, 120, doi:10.1002/2015JA021300, 2015.

33. Forbes, J.M., and X. Zhang, The Quasi-6-Day Wave and its Interactions with Solar Tides, J. Geophys. Res. Space Physics, 122, doi:10.1002/2017JA023954, 2017.

34. Tolson, R.H., Keating, G.M., Cancro, G.J., Parker, J.S., Noll, S.N., and Wilkerson, B.L., Application of Accelerometer Data to Mars Global Surveyor Aerobraking Operations, J. Spacecr. Rockets, 36(3), 323–329, 1999.

35. Tolson, R.H., Dwyer, A.M., Hanna, J.L., Keating, G.M., George, B.E., Escalera, P.E., and Werner, M.R., Applications of Accelerometer Data to Mars Odyssey Aerobraking and Atmospheric Modeling, J. Spacecr. Rockets, 42(3), 435–443, 2005

36. Tolson, R., E. Bemis, S. Hough, K. Zaleski, G. Keating, J. Shidner, S. Brown, A. Brickler, M. Scher, and P. Thomas, Atmospheric modeling using accelerometer data during Mars Reconnaissance Orbiter aerobraking operations, J. Spacecr. Rockets, 45, 511–518, doi:10.2514/1.34301, 2008.

37. Zurek, R.W., R.A. Tolson, S.W. Bougher, R.A. Lugo, D.T. Baird, J.M. Bell, and B.M. Jakosky, Mars thermosphere as seen in MAVEN accelerometer data, J. Geophys. Res. Space Physics, 122, doi:10.1002/2016JA023641, 2017.

38. England, S. L., et al., Simultaneous observations of atmospheric tides from combined in situ and remote observations at Mars from the MAVEN spacecraft, J. Geophys. Res. Planets, 121, doi:10.1002/2016JE004997, 2016.

39. Liu, G., S. England, R. J. Lillis, P. R. Mahaffy, M. Elrod, M. Benna, and B. Jakosky, Longitudinal structures in Mars' upper atmosphere as observed by MAVEN/NGIMS, J. Geophys. Res. Space Physics, 122, 1258–1268, doi:10.1002/2016JA023455, 2017.

40. Moudden Y., J. M. Forbes, Topographic connections with density waves in Mars' aerobraking regime, J. Geophys. Res., 113, E11009, doi:10.1029/2008JE003107, 2008.

41. Palo, S.E., Roble, R.G., and M.E. Hagan, Middle atmosphere effects of the quasi-two-day wave determined from a General Circulation Model, Earth Planets Space, 51, 629-647, 1999.

42. Nguyen, V.A., S.E. Palo, R.S. Liebermann, J.M. Forbes, D.A. Ortland, and D.E. Siskind, Generation of secondary waves arising from nonlinear interaction between the quasi 2-day wave and the migrating diurnal tide, J. Geophys. Res., 121, 7762–7780, doi:10.1002/2016JD024794, 2016.

43. Pedatella, N.M., H.-L. Liu, and M.E. Hagan, Day-to-day migrating and nonmigrating tidal variability due to the six-day planetary wave, J. Geophys. Res., 117, A06301, doi:10.1029/2012JA017581, 2012.

44. Hagan, M.E., A. Maute, and R.G. Roble (2009), Tropospheric tidal effects on the middle and upper atmosphere, J. Geophys. Res., 114, A01302, doi:10.1029/2008JA013637.

45. Yamashita, K., S. Miyahara, Y. Miyoshi, K. Kawano, and J. Ninomiya, Seasonal variation of non-migrating semidiurnal tide in the polar MLT region in a general circulation model, J. Atmos. Sol. Terr. Phys., 64, 1083–1094, 2002.

46. Angelats i Coll, M., and J.M. Forbes, Nonlinear interactions in the upper atmosphere: The s = 1 and s = 3 nonmigrating semidiurnal tides, J. Geophys. Res., 107(A8), 1157, doi:10.1029/2001JA900179, 2002.

47. Liu, H.-L., W. Wang, A. D. Richmond, and R. G. Roble, Ionospheric variability due to planetary waves and tides for solar minimum conditions, J. Geophys. Res., 115, A00G01, doi:10.1029/2009JA015188, 2010.

48. Chang, L.C., S.E. Palo, and H.-L. Liu, Short-term variation of the s = 1 nonmigrating semidiurnal tide during the 2002 stratospheric sudden warming, J. Geophys. Res., 114, D03109, doi:10.1029/ 2008JD010886, 2009.

49. Lieberman, R.S., J. Oberheide, M.E. Hagan, E.E. Remsberg and L.L. Gordley, Variability of diurnal tides and planetary waves during November 1978 - May 1979, J. Atmos. Solar-Terr. Phys., 66, 517-528, 2004.

50. Lieberman, R.S., D.M. Riggin, D.A. Ortland, J. Oberheide, and D.E. Siskind, Global observations and modeling of nonmigrating diurnal tides generated by tide-planetary wave interactions, J. Geophys. Res. Atmos., 120, 11,419–11,437, doi:10.1002/ 2015JD023739, 2015.

51. Pedatella, N.M., and J.M. Forbes, Evidence for stratosphere sudden warming-ionosphere coupling due to vertically propagating tides, Geophys. Res. Lett., 37, L11104, doi:10.1029/2010GL043560, 2010.

52. Pancheva, D., P. Mukhtarov, and B. Andonov, Nonmigrating tidal activity related to the sudden stratospheric warming in the Arctic winter of 2003/2004, Ann. Geophys., 27, 975–987, 2009.